

OPEN ACCESS

A polaritonic two-component Bose–Hubbard model

To cite this article: M J Hartmann *et al* 2008 *New J. Phys.* **10** 033011

View the [article online](#) for updates and enhancements.

You may also like

- [Bose–Hubbard dynamics of polaritons in a chain of circuit quantum electrodynamics cavities](#)
Martin Leib and Michael J Hartmann
- [Exciton-polariton trapping and potential landscape engineering](#)
C Schneider, K Winkler, M D Fraser et al.
- [Polariton lasers. Hybrid light–matter lasers without inversion](#)
Daniele Bajoni

A polaritonic two-component Bose–Hubbard model

M J Hartmann^{1,2,3}, F G S L Brandão^{1,2}
and M B Plenio^{1,2}

¹ Institute for Mathematical Sciences, Imperial College London,
53 Exhibition Road, SW7 2PE, UK

² QOLS, The Blackett Laboratory, Imperial College London,
Prince Consort Road, SW7 2BW, UK

E-mail: m.hartmann@imperial.ac.uk

New Journal of Physics **10** (2008) 033011 (12pp)

Received 8 December 2007

Published 6 March 2008

Online at <http://www.njp.org/>

doi:10.1088/1367-2630/10/3/033011

Abstract. We demonstrate that polaritons in an array of interacting micro-cavities with strong atom–photon coupling can form a two-component Bose–Hubbard model in which both polariton species are protected against spontaneous emission as their atomic part is stored in two ground states of the atoms. The parameters of the effective model can be tuned via the driving strength of external lasers and include attractive and repulsive polariton interactions. We also describe a method to measure the number statistics in one cavity for each polariton species independently.

³ Author to whom any correspondence should be addressed.

Contents

| | |
|--|-----------|
| 1. Introduction | 2 |
| 2. The basic setting | 3 |
| 3. The atoms | 3 |
| 4. Polaritons | 4 |
| 5. Perturbations | 5 |
| 6. Polariton tunnelling | 6 |
| 7. Parameter range | 7 |
| 8. Numerical results | 7 |
| 9. Experimental realizability | 8 |
| 10. Measurements | 9 |
| 11. Summary | 10 |
| Acknowledgments | 10 |
| Appendix. The relevant dressed states | 11 |
| References | 12 |

1. Introduction

In recent years, significant progress in the theoretical and experimental study of quantum many-body phenomena has been made by employing artificial structures that permit unprecedented experimental control and measurement access. Early activity in this field in arrays of Josephson junctions [1] and was followed by several important developments with ultracold atoms in optical lattices [2]. Despite their success, Josephson junction arrays and optical lattices face limitations as it is challenging to access and control individual lattice sites, due to their small separation.

A possibility to overcome these hurdles has very recently been suggested in arrays of coupled micro-cavities, where a scheme for simulating the Bose–Hubbard Hamiltonian [3] and, subsequently, models of interacting Jaynes–Cummings Hamiltonians [4] have been studied. The phase diagrams of these models were studied [5, 6] and the existence of a glassy phase has been predicted [6]. These set-ups, where atoms interact with the resonant modes of the cavities, also offer the possibility to generate effective spin Hamiltonians [7] which, among many other applications, may be used for cluster state generation.

Here, we show that coupled high-Q cavities can host an effective two-component Bose–Hubbard model,

$$\begin{aligned}
 H = \sum_{\vec{R}; j=b,c} \mu_j n_{\vec{R}}^{(j)} - \sum_{\langle \vec{R}, \vec{R}' \rangle; j,l=b,c} J_{j,l} \left(j_{\vec{R}}^{\dagger} l_{\vec{R}'} + \text{h.c.} \right) + \sum_{\vec{R}; j=b,c} U_j n_{\vec{R}}^{(j)} \left(n_{\vec{R}}^{(j)} - 1 \right) \\
 + \sum_{\vec{R}} U_{b,c} n_{\vec{R}}^{(b)} n_{\vec{R}}^{(c)}, \tag{1}
 \end{aligned}$$

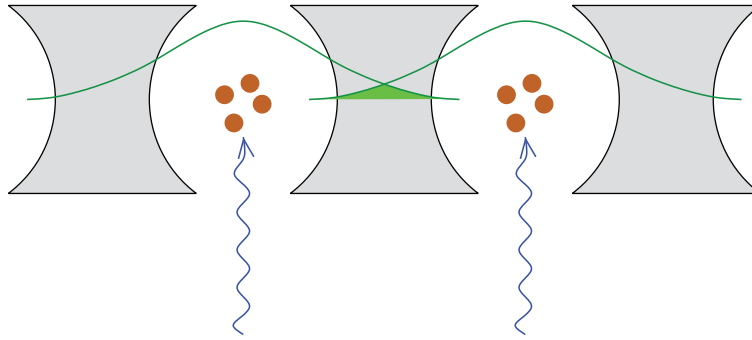


Figure 1. An array of cavities as described by our model. Photon hopping occurs due to the overlap (shaded green) of the light modes (green lines) of adjacent cavities. Atoms in each cavity (brown), which are driven by external lasers (blue) give rise to an on site potential.

where $b_{\vec{R}}^{\dagger}(c_{\vec{R}}^{\dagger})$ create polaritons of the type $b(c)$ in the cavity at site \vec{R} , $n_{\vec{R}}^{(b)} = b_{\vec{R}}^{\dagger}b_{\vec{R}}$ and $n_{\vec{R}}^{(c)} = c_{\vec{R}}^{\dagger}c_{\vec{R}}$. μ_b and μ_c are the polariton energies, U_b, U_c and $U_{b,c}$ their on-site interactions and $J_{b,b}, J_{c,c}$ and $J_{b,c}$ their tunnelling rates.

Bose–Hubbard models of two components can display several interesting phenomena which are partly also known for a Luttinger liquid of low energy excitations in fermionic systems [8]. Among these are spin density separation [9], spin order in the Mott regime [10] and phase separation [11].

2. The basic setting

For the realization of the Hamiltonian (1), we consider an array of cavities which are coupled via photon hopping (cf figure 1). We study the dynamics of polaritons, combined atom–photon excitations, in this arrangement. The interaction between two polaritons occupying the same cavity is generated by a large Kerr nonlinearity [12, 13]. This interaction can be repulsive and attractive. In each cavity, the resonant mode interacts with an ensemble of atoms, which are driven by an external laser, to form the polaritons. By varying the intensity of the driving laser, the parameters of the effective model (1) can be tuned. Since the distance between adjacent cavities is considerably larger than the optical wavelength of the resonant mode, individual sites can be controlled and measured with optical lasers. An experimental realization would require cavities that operate in the strong coupling regime [14]–[19].

3. The atoms

The interaction between polaritons that are located in the same cavity is generated by a nonlinearity in 4 level atoms with a level structure shown in figure 2 which was initially discovered by Imamoğlu *et al* [12]. The transitions between levels 2 and 3 are coupled to a laser and the transitions between levels $2 \leftrightarrow 4$ and $1 \leftrightarrow 3$ couple via dipole moments to the cavity resonance mode.

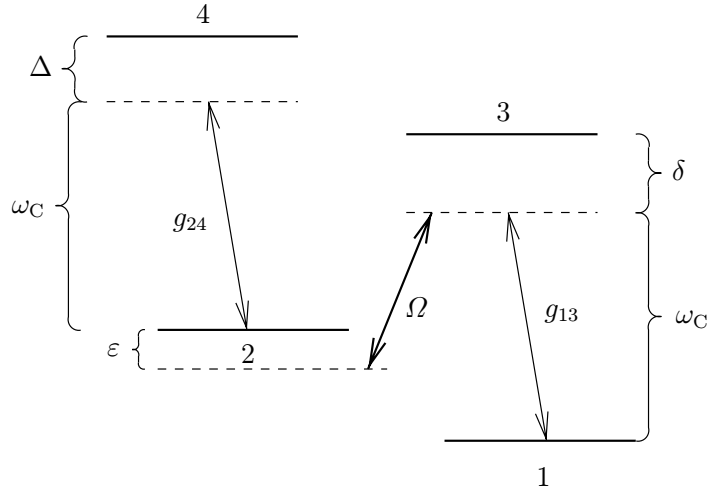


Figure 2. The level structure and transitions of one atom, ω_C is the frequency of the cavity mode, Ω is the Rabi frequency of the driving laser, g_{13} and g_{24} are dipole couplings to the cavity mode and δ , Δ and ε are detunings.

In a rotating frame with respect to $H_0 = \omega_C(a^\dagger a + \frac{1}{2}) + \sum_{j=1}^N (\omega_C \sigma_{22}^j + \omega_C \sigma_{33}^j + 2\omega_C \sigma_{44}^j)$, the Hamiltonian of the atoms in the cavity reads,

$$H_I = \sum_{j=1}^N (\varepsilon \sigma_{22}^j + \delta \sigma_{33}^j + (\Delta + \varepsilon) \sigma_{44}^j) + \sum_{j=1}^N (\Omega \sigma_{23}^j + g_{13} \sigma_{13}^j a^\dagger + g_{24} \sigma_{24}^j a^\dagger + \text{h.c.}), \quad (2)$$

where $\sigma_{kl}^j = |k_j\rangle\langle l_j|$ transfers level l of atom j to level k of the same atom, ω_C is the frequency of the cavity mode, δ , Δ and ε are detuning parameters (see figure 2), Ω is the Rabi frequency of the classical control laser and g_{13} and g_{24} are the parameters of the dipole coupling of the cavity mode to the respective atomic transitions which are all assumed to be real. All atoms interact in the same way with the cavity mode and hence the only relevant states are Dicke-type dressed states which we present in the appendix⁴. In the following derivation, all operator equations are only meant to hold for the matrix elements of the operators in the subspace spanned by the states (A.1)–(A.11).

4. Polaritons

In the case where $g_{24} = 0$ and $\varepsilon = 0$, the Hamiltonian H_I can be written in terms of three species of polaritons, p_0^\dagger , p_+^\dagger and p_-^\dagger . It takes on the form,

$$[H_I]_{g_{24}=0, \varepsilon=0} = \mu_0 p_0^\dagger p_0 + \mu_+ p_+^\dagger p_+ + \mu_- p_-^\dagger p_-. \quad (3)$$

⁴ If the atoms were distributed on fixed positions in space, the dressed states are no longer symmetric but the approach still works exactly the same.

The creation (and annihilation) operators read,

$$p_0^\dagger = \frac{1}{B} \left(g S_{12}^\dagger - \Omega a^\dagger \right) \quad \text{and} \quad p_\pm^\dagger = \sqrt{\frac{2}{A(A \pm \delta)}} \left(\Omega S_{12}^\dagger + g a^\dagger \pm \frac{A \pm \delta}{2} S_{13}^\dagger \right), \quad (4)$$

where $g = \sqrt{N} g_{13}$, $B = \sqrt{g^2 + \Omega^2}$, $A = \sqrt{4B^2 + \delta^2}$, $S_{12}^\dagger = \frac{1}{\sqrt{N}} \sum_{j=1}^N \sigma_{21}^j$ and $S_{13}^\dagger = \frac{1}{\sqrt{N}} \sum_{j=1}^N \sigma_{31}^j$. The frequencies of the polaritons p_0^\dagger , p_+ and p_- are given by $\mu_0 = 0$ and $\mu_\pm = (\delta \pm A)/2$. In the relevant Hilbert space spanned by symmetric Dicke-type dressed states (A.1)–(A.11) and for $N \gg 1$, they satisfy bosonic commutation relations,

$$[p_j, p_l] = 0 \quad \text{and} \quad [p_j, p_l^\dagger] = \delta_{jl} \quad \text{for } j, l = 0, +, -, \quad (5)$$

where the neglected terms are of order ‘number of polaritons’ / N . p_0^\dagger , p_+ and p_- thus describe independent bosonic particles.

We will now consider the case $\delta \gg \Omega, g$. Here, the polaritons and their frequencies read,

$$\begin{aligned} p_0^\dagger &= \frac{1}{B} \left(g S_{12}^\dagger - \Omega a^\dagger \right), & \mu_0 &= 0, \\ p_-^\dagger &\approx \frac{1}{B} \left(\Omega S_{12}^\dagger + g a^\dagger \right) - \frac{B}{\delta} S_{13}^\dagger, & \mu_- &= -\frac{B^2}{\delta}, \\ p_+^\dagger &\approx S_{13}^\dagger + \frac{1}{\delta} \left(\Omega S_{12}^\dagger + g a^\dagger \right), & \mu_+ &= \delta + \frac{B^2}{\delta}, \end{aligned} \quad (6)$$

up to first order in δ^{-1} . There is no spontaneous emission from the atomic level 2 and hence to leading order, the polaritons p_0^\dagger and p_-^\dagger do not experience spontaneous emission loss. We therefore define the two polariton species

$$b^\dagger = \frac{1}{B} \left(g S_{12}^\dagger - \Omega a^\dagger \right) \quad \text{and} \quad c^\dagger = \frac{1}{B} \left(\Omega S_{12}^\dagger + g a^\dagger \right). \quad (7)$$

In the rotating frame, the polaritons b^\dagger have an energy $\mu_b = 0$ and the polaritons c^\dagger have an energy $\mu_c = -B^2/\delta$. A possible disorder in the resonance frequency of the cavities and hence in δ would thus affect μ_b and μ_c differently which can have interesting consequences for the phase transitions of the model [20]. The dynamics of these two species is governed by the two component Bose–Hubbard Hamiltonian (1) as we shall see.

The Zeeman quantum numbers of atomic levels 1 and 2 can either be the same or differ by 2. In the latter case, the polaritons p_0^\dagger and p_-^\dagger can have magnetic moments [21]. Assuming that the atomic cloud in a cavity has the diameter of an optical wavelength, we estimate the exchange energy of the magnetic dipole–dipole interaction to be ~ 1 Hz. This is significantly smaller than all parameters of (1) and can thus be neglected in our approach.

5. Perturbations

To write the full Hamiltonian H_I , in the polariton σ basis, we express the operators $\sum_{j=1}^N \sigma_{22}^j$ and $a^\dagger \sum_{j=1}^N \sigma_{24}^j$ in terms of b^\dagger , c^\dagger and p_+^\dagger . In the subspace spanned by the states (A.1)–(A.11), we have $\sum_{j=1}^N \sigma_{22}^j = S_{12}^\dagger S_{12}$ and $\sum_{j=1}^N \sigma_{24}^j = S_{12}^\dagger S_{14}$, where $S_{14}^\dagger = \frac{1}{\sqrt{N}} \sum_{j=1}^N \sigma_{41}^j$. We thus obtain,

$$\sum_{j=1}^N \sigma_{42}^j a \approx -S_{14}^\dagger \left(g \Omega (c^2 - b^2) + (g^2 - \Omega^2) b c \right) / B^2, \quad (8)$$

where we made use of a rotating wave approximation: since $\delta \gg \Omega, g$, couplings to the polaritons p_+^\dagger can be neglected, provided that

$$|g_{24}|, |\varepsilon|, |\Delta| \ll |\mu_+ - \mu_b|, |\mu_+ - \mu_c|. \quad (9)$$

This is because all couplings between p_+^\dagger and b^\dagger or c^\dagger are much too weak to overcome the energy differences $|\mu_+ - \mu_b|$ and $|\mu_+ - \mu_c|$ between p_+^\dagger and b^\dagger or c^\dagger .

For $\max(|g_{24}g\Omega/B^2|, |g_{24}(g^2 - \Omega^2)/B^2|) \ll |\Delta|$, the couplings to level 4 can be treated in a perturbative way. If furthermore $|g_{24}g\Omega/B^2| \ll |B^2/\delta|$, this results in energy shifts of $n_b(n_b - 1)U_b, n_c(n_c - 1)U_c$ and $n_b n_c U_{bc}$, where n_b and n_c are the numbers of b^\dagger and c^\dagger polaritons respectively. The on-site interactions for the polaritons b^\dagger and c^\dagger can thus be written as⁵,

$$U_b b^\dagger b (b^\dagger b - 1) + U_c c^\dagger c (c^\dagger c - 1) + U_{bc} b^\dagger b c^\dagger c \quad (10)$$

with

$$U_b = -\frac{g_{24}^2 g^2 \Omega^2}{B^4 \Delta}, \quad (11)$$

$$U_c = -\frac{g_{24}^2 g^2 \Omega^2}{B^4 (\Delta + 2B^2/\delta)} \quad (12)$$

and

$$U_{bc} = -\frac{g_{24}^2 (g^2 - \Omega^2)^2}{B^4 (\Delta + B^2/\delta)}. \quad (13)$$

Note that $U_b > 0$ if $\Delta < 0$, $U_c > 0$ if $\Delta + 2B^2/\delta < 0$, $U_{bc} > 0$ if $\Delta + B^2/\delta < 0$ and vice versa. There can thus be repulsive and attractive interactions at the same time, e.g. for $\Delta < 0$ and $|\Delta| < B^2/\delta$ we have $U_b > 0$, $U_c < 0$ and $U_{bc} < 0$. In a similar way, the two photon detuning ε leads to an additional on-site term

$$\frac{\varepsilon}{B^2} (g^2 b^\dagger b + \Omega^2 c^\dagger c + g\Omega (b^\dagger c + c^\dagger b)), \quad (14)$$

where the transitions $b^\dagger c + c^\dagger b$ are suppressed if $|\varepsilon g\Omega/B^2| \ll |B^2/\delta|$.

6. Polariton tunnelling

If the cavities are either coupled by optical fibre tapers or directly via an overlap of evanescent fields, photons can tunnel between neighbouring cavities. This process is described by the Hamiltonian $\alpha (a_{\bar{R}}^\dagger a_{\bar{R}'} + \text{h.c.})$ with the photon tunnelling rate α . We translate this term into the polariton picture and assume that the tunnelling rate is much smaller than δ . In this regime, the tunnelling does not induce transitions between the polaritons b^\dagger or c^\dagger and p_+^\dagger . Hence the p_+^\dagger decouple from the polaritons b^\dagger and c^\dagger whose tunnelling terms read,

$$J_{bb} b_{\bar{R}}^\dagger b_{\bar{R}'} + J_{cc} c_{\bar{R}}^\dagger c_{\bar{R}'} - J_{bc} (b_{\bar{R}}^\dagger c_{\bar{R}'} + c_{\bar{R}}^\dagger b_{\bar{R}'}) + \text{h.c.}, \quad (15)$$

where

$$J_{bb} = \alpha g^2 / B^2, \quad (16)$$

$$J_{cc} = \alpha \Omega^2 / B^2 \quad (17)$$

⁵ For $|g_{24}g\Omega/B^2| > |B^2/\delta|$, an additional term $-g_{24}^2 g^2 \Omega^2 B^{-4} \Delta^{-1} (c^\dagger c^\dagger b b + b^\dagger b^\dagger c c)$ arises.

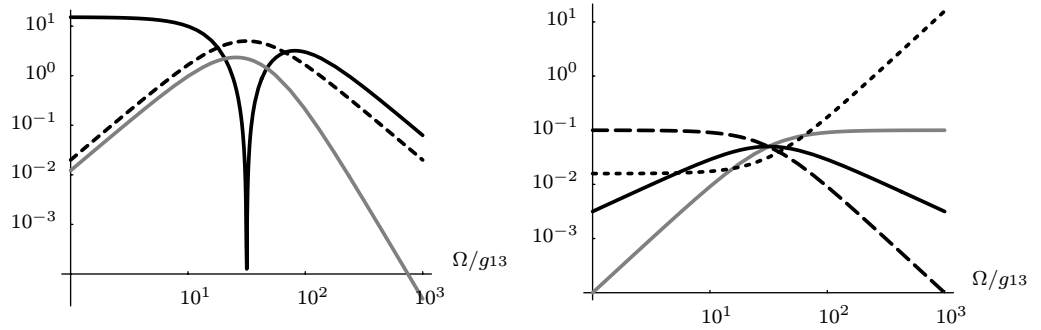


Figure 3. Left: the polariton interactions U_b (dashed line), U_c (grey line) and U_{bc} (solid line) in units of g_{13} as a function of Ω/g_{13} . Right: the tunnelling rates $|J_{bb}|$ (dashed line), $|J_{cc}|$ (grey line) and $|J_{bc}|$ (solid line) together with $|\mu_c - \mu_b|$ (dotted line) in units of g_{13} as a function of Ω/g_{13} . The parameters of the system are $g_{24} = g_{13}$, $N = 1000$, $\delta = -g_{13}/20$, $\delta = 2000\sqrt{N}g_{13}$ and $\alpha = g_{13}/10$.

and

$$J_{bc} = \alpha g \Omega / B^2. \quad (18)$$

If $|J_{bc}| \ll |B^2/\delta|$, transitions between b^\dagger and c^\dagger are suppressed. This is the case for any Ω as long as $g^2 \gg \alpha\delta/2$.

7. Parameter range

Here, we give one example of how the parameters of the effective Hamiltonian (1) vary as a function of the intensity of the driving laser Ω . We choose the parameters of the atom cavity system to be $g_{24} = g_{13}$, $N = 1000$, $\Delta = -g_{13}/20$, $\delta = 2000\sqrt{N}g_{13}$ and $\alpha = g_{13}/10$. Figure 3 shows the interactions U_b , U_c and U_{bc} , the tunnelling rates J_{bb} , J_{cc} and J_{bc} and $|\mu_c - \mu_b|$ as a function of Ω/g_{13} . For $g \approx \Omega$, we have $|U_{bc}| \ll |U_b|, |U_c|$ and $J_{bb} \approx J_{cc} \approx J_{bc}$. Whenever $|\mu_c - \mu_b| < |J_{bc}|$, b^\dagger polaritons get converted into c^\dagger polaritons and vice versa via the tunnelling J_{bc} . With the present choice of α and δ , this happens for $0.16g < \Omega < 1.6g$. To avoid such processes, one either needs to choose α smaller or δ larger, where both choices would require higher Q of the cavities to ensure sufficient lifetime. The interactions U_b , U_c and U_{bc} can furthermore be adjusted by varying the detuning Δ . This can be done by generating a Stark shift to the atomic level 4 with an additional laser that drives the transition between level 4 and a further atomic level in a dispersive (detuned) way.

8. Numerical results

To confirm the validity of the approximations involved in the above derivation, we present a numerical simulation of the full dynamics of polaritons b^\dagger and c^\dagger in three cavities that each couple to $N = 1000$ atoms and compare it to the dynamics of the corresponding effective model (1). We consider initial conditions with exactly one polariton b^\dagger in cavities 1 and 2 and exactly one polariton c^\dagger in cavity 3. Figure 4(a) shows the numbers $N_b = \langle n_b \rangle$ and $N_c = \langle n_c \rangle$ of polaritons b^\dagger and c^\dagger and their number fluctuations $F_b = \langle n_b^2 \rangle - N_b^2$ and $F_c = \langle n_c^2 \rangle - N_c^2$ for

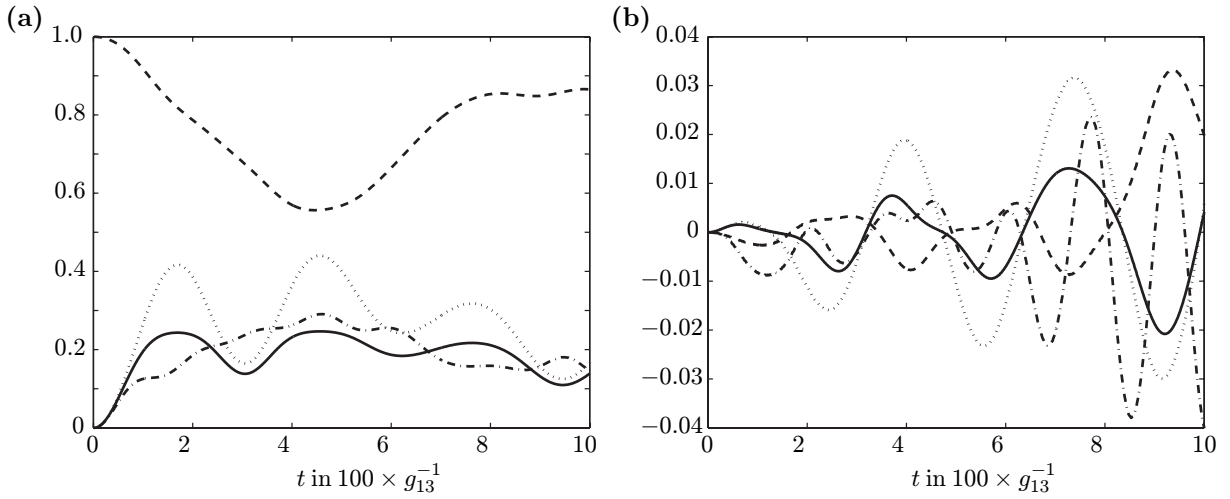


Figure 4. (a) N_b (dotted line), N_c (dashed line), F_b (solid line) and F_c (dash-dotted line) for a full model of 3 cavities with $g_{24} = g_{13}$, $\varepsilon = 0$, $N = 1000$, $\Omega = \frac{3}{2}\sqrt{N}g_{13}$, $\delta = 10^4 g_{13}$, $\Delta = -46g_{13}$ and $\alpha = 2.2 \times 10^{-3} g_{13}$. (b) Differences between the full and the effective description, $[N_b]_{\text{full}} - [N_b]_{\text{BH}}$ (dotted line), $[N_c]_{\text{full}} - [N_c]_{\text{BH}}$ (dashed line), $[F_b]_{\text{full}} - [F_b]_{\text{BH}}$ (solid line) and $[F_c]_{\text{full}} - [F_c]_{\text{BH}}$ (dash-dotted line) for the same model.

the first cavity. Figure 4(b) in turn shows differences between the full description and the effective model (1), $[N_b]_{\text{full}} - [N_b]_{\text{BH}}$, $[N_c]_{\text{full}} - [N_c]_{\text{BH}}$, $[F_b]_{\text{full}} - [F_b]_{\text{BH}}$ and $[F_c]_{\text{full}} - [F_c]_{\text{BH}}$. The effective model describes the dynamics very well.

9. Experimental realizability

To analyse the model's experimental realizability, possible decay mechanisms for the polaritons need to be considered. Level 2 of the atoms is metastable and hence its decay rate is negligible on the relevant timescales. The decay mechanisms for the polaritons b^\dagger and c^\dagger thus originate in the cavity decay of the photons and the very small but non-negligible occupations of the excited levels 3 and 4. The occupation of level 4 is due to the coupling $\sum_{j=1}^N (\sigma_{42}^j a + \text{h.c.})$, whereas the occupation of level 3 only affects the polaritons c^\dagger and stems from the linear correction term $-(B/\delta)S_{13}^\dagger$ in equation (6). The resulting effective decay rates, Γ_b for the polaritons b^\dagger and Γ_c for the polaritons c^\dagger , read

$$\Gamma_b = \frac{\Omega^2}{B^2} \kappa + \Theta(n_b - 2) \frac{g_{24}^2 g^2 \Omega^2}{\Delta^2 B^4} \gamma_4, \quad (19)$$

$$\Gamma_c = \frac{g^2}{B^2} \kappa + \frac{B^2}{\delta^2} \gamma_3 + \Theta(n_c - 2) \frac{g_{24}^2 g^2 \Omega^2}{\Delta^2 B^4} \gamma_4, \quad (20)$$

where Θ is the Heaveside step function, κ the cavity decay rate and γ_3 (γ_4) the spontaneous emission rates from levels 3 (4). For successfully observing the dynamics and phases of effective Hamiltonian (1), the interactions U_b , U_c and U_{bc} need to be much larger than Γ_b and Γ_c .

The experimentally least demanding case is the one-component model for the polaritons b^\dagger , for which $\delta \sim g$. Assuming $g_{24} = g_{13}$ the maximal achievable ratio of U_b/Γ_b is here $\frac{1}{2} g_{13}/\sqrt{\kappa \Theta(n_b - 2)\gamma_4}$. In particular the Mott state for the polaritons b^\dagger , where $n_b < 2$, can even be realized in bad cavities without the strong coupling regime. However, to observe the transition to the superfluid phase, the strong coupling regime with $g_{13} \gg \sqrt{\kappa\gamma_4}$ is required for the single component model, too.

To obtain an estimate for a model with both components, b^\dagger and c^\dagger , we consider three cases, $g \approx \omega$, $\Omega \approx 10g$ and $\Omega \approx g/10$. Note that $g \ll \delta$ and hence spontaneous emission via level 3 is strongly suppressed. Denoting $\zeta = g_{13}/\sqrt{\kappa\gamma_4}$, the achievable ratios of interaction versus decay rates for $g \approx \Omega$ are $U_b/\Gamma_b \approx U_c/\Gamma_c \approx \zeta/(2\sqrt{2})$, while the cross interaction vanishes, $U_{bc} \approx 0$. For $\Omega = 10g$ ($\Omega = g/10$) the achievable ratios are $U_b/\Gamma_b \approx \zeta/100$ ($U_b/\Gamma_b \approx \zeta/2$), $U_c/\Gamma_c \approx \zeta/2$ ($U_c/\Gamma_c \approx \zeta/100$) and $U_{bc}/\max(\Gamma_b, \Gamma_c) \approx \zeta$ ($U_{bc}/\max(\Gamma_b, \Gamma_c) \approx \zeta$).

Realizing these parameters requires cavities that operate in the strong coupling regime with large cooperativity factors, $\zeta \gg 1$. This regime is currently being achieved in several devices, in BECs coupled to fibre-based cavities [14] ($\zeta \approx 17$), photonic band gap cavities [15] ($\zeta \approx 8$), Fabry–Perot cavities [16] ($\zeta \approx 13$), toroidal micro-cavities [17] ($\zeta \approx 7$) and micro-cavities on a gold coated silicon chip [18] ($\zeta \approx 6$) among others. Our scheme should thus be experimentally feasible with current or soon to be available technology. Values of ζ that are predicted to be achievable are as high as 200 for photonic bandgap cavities and 3000 for toroidal micro-cavities [19].

Besides the strong coupling itself, a realization of our scheme also requires that the atoms remain in the location of strong coupling for sufficient time. The parameters of the effective Hamiltonian (1) are at most two or three orders of magnitude smaller than the atom–photon coupling g_{13} , see figure 3. Currently strong coupling regimes with $g_{13} \approx 10$ GHz are achieved, which requires an atom–photon interaction time of microseconds to be able to observe the interesting dynamics. This time is sufficient for driving the system through phase transitions (see also figure 4 in [3] for a simulation of the one component case) and is even achieved with falling atoms [17]. Trapping times for cold atoms exceed this timescale by far [22].

Another limiting factor could be the thermal motion of trapped atoms. If one requires that an atom should not move more than 100 nm in 1 μ s, the temperature of the atoms needs to be $\sim 10^{-4}$ K which is routinely realized in cold atom experiments.

10. Measurements

The number statistics of both polariton species b^\dagger and c^\dagger in one cavity can be measured using state selective resonance fluorescence in a way proposed in [23]. In the one-component BH model [3], the polaritons can therefore be mapped by a STIRAP passage [24] onto the atomic levels. In the two-component case, the STIRAP can however not be applied as in [3] because the energies μ_b and μ_c are similar and the passage would thus need to be extremely slow to be adiabatic.

For two components, one can do the measurements as follows. First the external driving laser Ω is switched off. Then the roles of atomic levels 1 and 2 are interchanged in each atom via a Raman transition by applying a $\pi/2$ -pulse. To this end the transitions $1 \leftrightarrow 3$ and $2 \leftrightarrow 3$ are driven with two lasers (both have the same Rabi frequency Λ) in two-photon resonance for a time $T = \pi \delta_\Lambda / |\Lambda|^2$ (δ_Λ is the detuning from atomic level 3). The configuration is shown in figure 5(a). This pulse results in the mapping $|1_j\rangle \leftrightarrow |2_j\rangle$ for all atoms j .

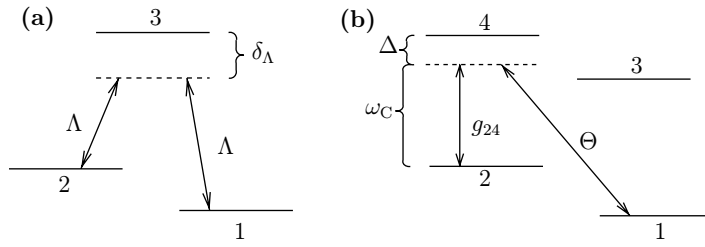


Figure 5. (a) Configuration of the $\pi/2$ -pulse. Two driving lasers in two-photon transition with identical Rabi frequencies Λ couple to the atomic transitions $1 \leftrightarrow 3$ and $2 \leftrightarrow 3$. (b) Configuration for the STIRAP process. A driving laser couples to the $1 \leftrightarrow 4$ transition with Rabi frequency Θ . The cavity mode couples to transitions $2 \leftrightarrow 4$ and $1 \leftrightarrow 3$, where the coupling to $1 \leftrightarrow 3$ is ineffective and not shown.

Next another laser, Θ , that drives the transition $1 \leftrightarrow 4$ is switched on, see figure 5(b). Together with the coupling g_{24} , this configuration can be described in terms of three polaritons, q_0^\dagger , q_+^\dagger and q_-^\dagger , in an analogous way to p_0^\dagger , p_+^\dagger and p_-^\dagger , where now the roles of the atomic levels 1 and 2 and the levels 3 and 4 are interchanged. Hence, if we choose $\Theta = \Omega$ the $\pi/2$ -pulse maps the b^\dagger onto the dark state polaritons of the new configuration, q_0^\dagger , whereas if we choose $\Theta = -\Omega$ it maps the c^\dagger onto q_0^\dagger . The driving laser is then adiabatically switched off, $\Theta \rightarrow 0$, and the corresponding STIRAP process maps the q_0^\dagger completely onto atomic excitations of level 1. This process can now be fast since the detuning Δ is significantly smaller than δ and hence the energies of all polariton species q_0^\dagger , q_+^\dagger and q_-^\dagger are well separated. Another $\pi/2$ -pulse finally maps the excitations of level 1 onto excitations of level 2, which can be measured by state selective resonance fluorescence in the same way as discussed in [3, 23].

The whole sequence of $\pi/2$ -pulse, STIRAP process and another $\pi/2$ -pulse can be done much faster than the timescale set by the dynamics of the Hamiltonian (1) [3] and b^\dagger or c^\dagger can be mapped onto atomic excitations in a time in which they are not able to move between sites. The procedure thus allows us to measure the instantaneous local particle statistics of each species separately.

11. Summary

We have shown that a two-component Bose–Hubbard model of polaritons can be created in coupled arrays of high- Q cavities. As new features, the model allows for single site addressing and can display transitions between the two particle species. An experimental realization is feasible with cavities that have cooperativity factors much greater than unity and interact with the atoms for sufficient time. The local particle number statistics of both species can be measured independently with high accuracy.

Acknowledgments

This work is part of the QIP-IRC supported by EPSRC (GR/S82176/0), the Integrated Project Qubit Applications (QAP) supported by the IST directorate as contract number 015848 and

was supported by the EPSRC grant EP/E058256/1, the Alexander von Humboldt Foundation, the Conselho Nacional de Desenvolvimento Científico e Tecnológico (CNPq) and the Royal Society.

Appendix. The relevant dressed states

For each cavity, we restrict our presentation here to the subspace which contains at most two excitations. The Hamiltonian (2) decouples into a zero excitation, a one excitation and a two excitation manifold. The zero excitation manifold consists of only one state $|\phi_0\rangle$, in which there is no photon and all atoms are in their ground state

$$|\phi_0\rangle = |0_{\text{photon}}\rangle \otimes \prod_{j=1}^N |1_j\rangle. \quad (\text{A.1})$$

There are three states in the one excitation manifold,

$$|\phi_1^a\rangle = |1_{\text{photon}}\rangle \otimes \prod_{j=1}^N |1_j\rangle, \quad (\text{A.2})$$

$$|\phi_1^b\rangle = |0_{\text{photon}}\rangle \otimes \frac{1}{\sqrt{N}} \sum_{j=1}^N |\dots 3_j \dots\rangle, \quad (\text{A.3})$$

$$|\phi_1^c\rangle = |0_{\text{photon}}\rangle \otimes \frac{1}{\sqrt{N}} \sum_{j=1}^N |\dots 2_j \dots\rangle, \quad (\text{A.4})$$

where $|\dots k_j \dots\rangle$ denotes the state where atom number j is in state $|k\rangle$ and all others are in state $|1\rangle$. The two excitation manifold contains seven states,

$$|\phi_2^a\rangle = |2_{\text{photon}}\rangle \otimes \prod_{j=1}^N |1_j\rangle, \quad (\text{A.5})$$

$$|\phi_2^b\rangle = |1_{\text{photon}}\rangle \otimes \frac{1}{\sqrt{N}} \sum_{j=1}^N |\dots 3_j \dots\rangle, \quad (\text{A.6})$$

$$|\phi_2^c\rangle = |1_{\text{photon}}\rangle \otimes \frac{1}{\sqrt{N}} \sum_{j=1}^N |\dots 2_j \dots\rangle, \quad (\text{A.7})$$

$$|\phi_2^d\rangle = |0_{\text{photon}}\rangle \otimes \frac{1}{\sqrt{2N(N-1)}} \sum_{j=1}^N \sum_{l \neq j}^N |\dots 3_j \dots 3_l \dots\rangle, \quad (\text{A.8})$$

$$|\phi_2^e\rangle = |0_{\text{photon}}\rangle \otimes \frac{1}{\sqrt{N}} \sum_{j=1}^N |\dots 4_j \dots\rangle, \quad (\text{A.9})$$

$$|\phi_2^f\rangle = |0_{\text{photon}}\rangle \otimes \frac{1}{\sqrt{N(N-1)}} \sum_{j=1}^N \sum_{l \neq j}^N |\dots 2_j \dots 3_l \dots\rangle, \quad (\text{A.10})$$

$$|\phi_2^g\rangle = |0_{\text{photon}}\rangle \otimes \frac{1}{\sqrt{2N(N-1)}} \sum_{j=1}^N \sum_{l \neq j} |\dots 2_j \dots 2_l \dots\rangle. \quad (\text{A.11})$$

Here, $|\dots 2_j \dots 2_l \dots\rangle$ denotes a state, where atom number j is in state $|2\rangle$, atom number l is in state $|3\rangle$ and the other atoms are all in the ground state.

References

- [1] Fazio R and van der Zant H S J 2001 *Phys. Rep.* **355** 235
- [2] Bloch I, Dalibard J and Zwerger W 2007 *Preprint* 0704.3011
- [3] Hartmann M J, Brandão F G S L and Plenio M B 2006 *Nat. Phys.* **2** 849
Hartmann M J and Plenio M B 2007 *Phys. Rev. Lett.* **99** 103601
- [4] Angelakis D G, Santos M F and Bose S 2007 *Phys. Rev. A* **76** 031805
Greentree A D, Tahan C, Cole J H and Hollenberg L C L 2006 *Nat. Phys.* **2** 856
- [5] Neil Na Y C, Utsunomiya S, Tian L and Yamamoto Y 2007 *Preprint* quant-ph/0703219
- [6] Rossini D and Fazio R 2007 *Phys. Rev. Lett.* **99** 186401
- [7] Hartmann M J, Brandão F G S L and Plenio M B 2007 *Phys. Rev. Lett.* **99** 160501
- [8] Haldane F D M 1981 *J. Phys. C: Solid State Phys.* **14** 2585
- [9] Recati A, Fedichev P O, Zwerger W and Zoller P 2003 *Phys. Rev. Lett.* **90** 020401
Kleine A, Kollath C, McCulloch I, Giamarchi T and Schollwoeck U 2007 *Preprint* 0706.0709
- [10] Duan L M, Demler E and Lukin M 2003 *Phys. Rev. Lett.* **91** 090402
Altman E, Hofstetter W, Demler E and Lukin M 2003 *New J. Phys.* **5** 113
Ziegler K 2003 *Phys. Rev. A* **68** 053602
- [11] Cazalilla M A and Ho A F 2003 *Phys. Rev. Lett.* **91** 150403
- [12] Imamoğlu A, Schmidt H, Woods G and Deutsch M 1997 *Phys. Rev. Lett.* **79** 1467
Imamoğlu A, Schmidt H, Woods G and Deutsch M 1998 *Phys. Rev. Lett.* **81** 2836
Werner M J and Imamoğlu A 1999 *Phys. Rev. A* **61** R011801
- [13] Brandão F G S L, Hartmann M J and Plenio M B 2007 *Preprint* 0704.2398
- [14] Colombe Y, Steinmetz T, Dubois G, Linke F, Hunger D and Reichel J 2007 *Nature* **450** 272
Steinmetz T, Colombe Y, Hunger D, Hnsch T W, Balocchi A, Warburton R J and Reichel J 2006 *Appl. Phys. Lett.* **89** 111110
- [15] Hennessy K, Badolato A, Winger M, Gerace D, Atature M, Gulde S, Falt S, Hu E L and Imamoglu A 2007 *Nature* **445** 896
- [16] Birnbaum K M, Boca A, Miller R, Boozer A D, Northup T E and Kimble H J 2005 *Nature* **436** 87–90
- [17] Aoki T, Dayan B, Wilcut E, Bowen W P, Parkins A S, Kimble H J, Kippenberg T J and Vahala K J 2006 *Nature* **443** 671
- [18] Trupke M, Hinds E A, Eriksson S, Curtis E A, Muktadir Z, Kukharenka E and Kraft M 2005 *Appl. Phys. Lett.* **87** 211106
- [19] Spillane S M, Kippenberg T J, Vahala K J, Goh K W, Wilcut E and Kimble H J 2005 *Phys. Rev. A* **71** 013817
- [20] Blagoeva E J, Nadjakov G, Busiello G, De Cesare L, Millev Y T, Rabuffo I and Uzunov D I 1990 *Phys. Rev. B* **42** 6124
- [21] Karpa L and Weitz M 2006 *Nat. Phys.* **2** 332
- [22] Chu S, Hollberg L, Bjorkholm J E, Cable A and Ashkin A 1985 *Phys. Rev. Lett.* **55** 48
- [23] Imamoğlu A 2002 *Phys. Rev. Lett.* **89** 163602
James D F V and Kwiat P G 2002 *Phys. Rev. Lett.* **89** 183601
- [24] Fleischhauer M, Imamoğlu A and Marangos J P 2005 *Rev. Mod. Phys.* **77** 633–73